International Journal of Nanomedicine Dovepress

Open Access Full Text Article ORIGINAL RESEARCH

Exosomes from Adipose-Derived Mesenchymal Stromal Cells Prevent Medication-Related Osteonecrosis of the Jaw by Inhibiting Macrophage M1 Polarization and Pyroptosis

Yi Zheng[1,2], Xinyu Wang[1], Yang He[1], Shuo Chen[1], Linhai He[1,3,*], Yi Zhang[1,*]

[1]Department of Oral and Maxillofacial Surgery, Peking University School and Hospital of Stomatology, Beijing, 100081, People's Republic of China; [2]Department of Stomatology, The First Affiliated Hospital, Zhejiang University School of Medicine, Hangzhou, 310003, People's Republic of China; [3]First Clinical Division, Peking University School and Hospital of Stomatology, Beijing, 100081, People's Republic of China

*These authors contributed equally to this work

Correspondence: Linhai He; Yi Zhang, Email helinhai07@126.com; zhangyi2000@263.net

Purpose: Exosomes from mesenchymal stromal cells (MSCs) can prevent the development of medication-related osteonecrosis of the jaw (MRONJ) by promoting tooth socket wound healing; however, the exact mechanism remains to be clarified. In this study, our aim was to explore the mechanisms of exosomes derived from adipose-derived mesenchymal stromal cells (ADSCs) in preventing MRONJ by focusing on macrophage M1 polarization and pyroptosis.

Methods: The MRONJ model was established by the administration of zoledronate and tooth extraction. Exosomes isolated from the supernatant of ADSCs were mixed with hydrogel and locally injected into the extraction site after tooth extraction. Stereoscope observations, micro computed tomography (microCT), and histological analysis were used to assess tooth socket wound healing.

Results: The results showed that exosomes could effectively avoid MRONJ via accelerating gingival wound healing and tooth socket bone regeneration. Mechanistically, zoledronate triggered the NF-κB signaling pathway and promoted p65 transferring into the nucleus in macrophages, resulting in macrophage M1 polarization and pyroptosis-mediated tissue inflammation, while exosomes could reduce macrophage pyroptosis and pro-inflammation cytokines release by suppressing the NF-κB/NLRP3/IL-1β axis. Additionally, IL-1RA derived from exosomes plays a key role in preventing MRONJ. Pyroptosis-related and inflammatory-related processes were upregulated in MRONJ patients further confirmed by assessing MRONJ gingival samples and healthy gingival tissues.

Conclusion: ADSCs-derived exosomes could effectively promote tooth socket healing and prevent MRONJ by inhibiting M1 macrophage activation and pyroptosis by blocking the NF-κB/NLRP3/IL-1β axis.

Keywords: Medication-related osteonecrosis of the jaw, exosomes, macrophage M1 polarization and pyroptosis, primary wound healing, NF-κB/NLRP3/IL-1β axis

Introduction

MRONJ is a rare and debilitating condition characterized by progressive bone destruction in the maxillofacial region in patients with a history of antiangiogenic or antiresorptive agents, which are commonly used to treat bone-metastatic cancers, Paget's disease, osteoporosis, multiple myeloma, and osteogenesis imperfecta.[1–3] The hypotheses of MRONJ pathophysiology include bone remodeling inhibition, angiogenesis inhibition, inflammation or infection, immune dysfunction, and genetic predisposition. However, these hypotheses have not been fully confirmed, and the pathogenesis of MRONJ still needs to be explored.[1,4] Also, the therapeutic efficiency remains limited.

Treatment of MRONJ typically involves surgical interventions and drug therapy. However, the success rate of surgical management is approximately 61–89%, and MRONJ may recur after surgery.[5] Recently, hyperbaric oxygen

Received: 28 August 2024
Accepted: 20 November 2024
Published: 26 November 2024

therapy, platelet-rich plasma, and low-level light therapy have been proven to be effective for MRONJ.[4] Currently, the optimal treatment for MRONJ has not been determined, and consensus on the sequential treatment of MRONJ still needs further study. MSCs therapy has been suggested as an alternative but effective option for MRONJ.[6–9] ADSCs are derived from adipose tissue and have advantages over other MSCs due to their rich sources, high yield, simple access, and little harm to the donor.[10,11] However, the clinical application of MSCs therapy raises some safety concerns, such as the risk of promoting tumor growth and metastasis.[12]

Emerging evidence has shown that paracrine signaling is the key mechanism of MSCs therapeutic efficacy to exert regenerative and immunomodulatory potential.[13] Exosomes (Exo) are important paracrine products of cell culture supernatant, which can transfer bioactive cargo to target cells, including nucleic acids, metabolites, proteins, and, lipids, mediating specific intracellular signaling pathways.[14–16] As Exo can move through body fluids like blood, saliva, and urine, reaching distant cells and tissues, they are considered an innovative strategy for tissue repair and regeneration.[17] Several studies have shown that MSCs-derived Exo effectively promote tooth socket wound healing and prevent MRONJ.[18,19] Our previous serial studies further suggested ADSCs and the Exo derived from ADSCs (ADSCs-Exo) successfully avoid MRONJ by promoting tooth socket wound healing.[20–22] However, the exact mechanism remains unclear.

Pyroptosis is a lytic and programmed cell death that is active by inflammasomes and performed by gasdermin proteins, which is associated with inflammation response.[23–25] Recently, macrophage pyroptosis has also drawn much concern in inflammation-related diseases.[26–28] Excessive macrophage pyroptosis and pro-inflammation factors production result in postponed wound healing and impaired tissue regeneration.[29,30] There is a close connection between macrophage M1 polarization and pyroptosis. The activation of M1 macrophages and the release of inflammatory mediators, like interleukin-1β (IL-1β), may induce pyroptosis.[31] In addition, macrophage M1 polarization and pyroptosis share some signaling pathways or regulatory mediators. For example, the TLR/NF-κB pathway not only plays an important role in macrophage M1 polarization, but also participates in the process of pyroptosis.[32,33] Studies have found that Exo can attenuate colitis[34] and inflammatory pain[35] and can repair ischemic muscle injury[36] by regulating macrophage pyroptosis. Thus, our study assessed the mechanisms of macrophage M1 polarization and pyroptosis in ADSCs-Exo-meditated gingival healing and prevention of MRONJ. These findings might contribute to clarifying the mechanisms of MRONJ and offer an alternative approach to the prevention of MRONJ.

Materials and Methods

Exosomes Isolation and Identification

The protocol for preparing ADSCs culture and Exo was as previously described.[20] Briefly, ADSCs were collected from the cell bank and cultured in α-modified Eagle medium with 10% fetal bovine serum (FBS) and 1% penicillin −streptomycin. ADSCs differentiation into osteogenic and adipogenic lineages and flow cytometry identification were described in supplementary methods. Exo were isolated from the supernatants of ADSCs by ultracentrifugation. The size and distribution of isolated Exo were measured with NTA. The morphology of isolated Exo was observed by TEM. Western blot was conducted to detect the main Exo markers (calnexin, CD63, and CD9). The hydrogel-exosome complex preparation was described in supplementary methods.

Cell Culture

BMDMs were prepared from the femur and tibia of male C57BL/6N mice (6-8-week-old), cultured in Roswell Park Memorial Institute (RPMI) 1640 medium with 10% FBS, 30 ng/mL M-CSF (576406, BioLegend, San Diego, CA, USA), and 1% penicillin−streptomycin. The cell viability test of Zol on BMDMs and exosomes uptake assay were described in supplementary methods. After reaching ~90% confluency, cells were pre-treated with Zol (25 μM, SML0223, Sigma, St. Louis, MO, USA) and/or Exo (100 μg/mL) or Raleukin (5 μg/mL, HY-108841, MCE, New Jersey, USA) for 24 h, after which they were stimulated with LPS (100 ng/mL, L2880, Escherichia coli, 055:B5, Sigma, St. Louis, MO, USA) for 4 h. For the MCC950 group, MCC950 (10 μM, No. S8930, Selleckchem, USA) was added for the final hour. Then, nigericin (10 μM, HY-100381, MCE, New Jersey, USA) was added for 1 h following LPS stimulation.

Flow Cytometry

Flow cytometry detected the surface markers. Briefly, BMDMs were cultured in 6-well cell culture plates. After incubation, BMDMs were collected and incubated with blocking antibody CD16/32 (B362118, Biolegend, San Diego, CA, USA) for 10 min and then with PE-CY7 anti-mouse CD86 (B360043, Biolegend, San Diego, CA, USA), PE anti-mouse CD206 (B347490, Biolegend, San Diego, CA, USA), BV421 anti-mouse F4/80 (B340005, Biolegend, San Diego, CA, USA), and APC anti-mouse CD11b (B336472, Biolegend, San Diego, CA, USA) antibodies for 30 min, then cells were washed and suspended in 300 μL phosphate buffer saline (PBS) with 1% FBS, after which flow cytometry was performed (Aria Sorp, BD, USA).

Cell Immunofluorescent Staining

BMDMs were cultured in 24-well plates. After incubation, cells were fixed with 4% paraformaldehyde (PFA) for 10 min and then incubated with 0.1% Triton X-100 for 15 min. Next, BMDMs were incubated with specific antibodies against iNOS (13120, CST, Boston, MA, USA), F4/80 (ab6640, Abcam, Cambridge, UK), NLRP3 (15101, CST, Boston, MA, USA), GSDMD (39754, CST, Boston, MA, USA), and P65 (8242, CST, Boston, MA, USA) at 4 °C overnight. BMDMs were then incubated with TRITC-conjugated (ZLI-0316, ZSGB-BIO, China) and/or FITC-conjugated secondary antibodies (ab96899, Abcam, Cambridge, UK) for 1 h at room temperature (RT). Next, cells were stained with 4′, 6-diamidino-2-phenylindole (DAPI) and assessed using an Olympus microscope.

RNA-Seq Analysis

Total RNA extraction and mRNA from clinical samples were enriched using TRIzol (Invitrogen, Thermo Fisher Scientific, USA) following the manufacturer's protocol. The clinical samples were sent to Beijing Allwegene Technology Co., Ltd. (Beijing, China) for the construction of the cDNA library. Illumina high-throughput sequencing platform (HiSeq 2500/4000) was used for RNA-seq. The raw reads obtained from Illumina sequencing (FASTQ format) were filtered to acquire clean reads by SOAPnuke. The following data mining and analysis, like KEGG, GO and PPI analysis, were carried out based on Dr. Tom Multi-omics mining system.

Western Blot

Western blot was conducted to analyze the proteins extracted from clinical samples, ADSCs, Exo, and BMDMs. Clinical gingival samples and cell lysates were obtained by sonication and centrifugation in RIPA lysis buffer (R0020, Solarbio, Beijing, China). BCA assay (23225, Thermo Fisher Scientific, USA) was used to measure the protein concentrations. Total proteins were separated on 10% SDS-PAGE gels and then transferred to polyvinylidene fluoride membranes (IPVH08100, Millipore, Germany). Then, block the membranes with 5% BSA for 1 h at RT, and incubate the membranes with primary antibodies against NLRP3 (15101, CST, Boston, MA, USA), cleaved-caspase-1 (89332, CST, Boston, MA, USA), caspase-1 (24232, CST, Boston, MA, USA), GSDMD (39754, CST, Boston, MA, USA), Phospho-NF-κB p659 (3033S, CST, Boston, MA, USA), IκBα (4812S, CST, Boston, MA, USA), Phospho-IκBα (2859S, CST, Boston, MA, USA), NF-κB p65 (8242S, CST, Boston, MA, USA), CD9 (ab263019; Abcam, Cambridge, UK), calnexin (ab133615, Abcam, Cambridge, UK), CD63 (ab134045, Abcam, Cambridge, UK), and β-Actin (TA-09, ZSGB-BIO, China) at 4 °C overnight. The next day, the membranes were incubated with HRP-conjugated secondary antibodies for 1 h at RT. Finally, samples were assessed using an ECL kit (P10300, NCM Biotech, Suzhou, China) using a Fusion system for imaging.

Enzyme-Linked Immunosorbent Assay (ELISA)

BMDMs culture supernatant was harvested, and the concentrations of tumor necrosis factor-α (TNF-α) (CSB-E04741m, Cusabio, Wuhan, China), IL-1β (432604, Biolegend, San Diego, CA, USA), and IL6 (E-EL-M0044c, Elabscience, Wuhan, China) were detected using ELISA kits under the manufacturer's instructions.

Animals

C57BL/6N male mice (6-8-week-old) were obtained from Beijing Vital River Laboratory Animal Technology Co., Ltd. All the animals were kept in specific pathogen-free facilities and given water and a regular diet *ad libitum*. All animal studies were authorized by the Ethics Committee of the Peking University Health Science Center (Permit number: LA2018017) and done in compliance with the regulations and guidelines of the Peking University Institutional Animal Care and Use Committee and ARRIVE guidelines. The mice were left in their cages for 1 week to familiarize themselves with their environment.

MRONJ Mouse Model

The mice were randomly assigned to four groups, with five mice in each group: (1) Ctrl group: administration of 0.9% NaCl saline (Veh) once a day; (2) Zol group: administration of Zol (1mg/kg) once a day; (3) Hydrogel group: administration of Zol once a day; (4) Exo group (100 μg/mL, 2–3 μL): administration of Zol once a day. Zol was administrated intraperitoneally (i.p). Once a day for four weeks to build the MRONJ model. Under general anesthesia by i.p. injection of pentobarbital (50 mg/kg), the mice's maxillary first molars were extracted after two weeks of Zol administration. Then, PBS, hydrogel, and hydrogel-Exo complex were injected locally into the extraction site respectively of the Zol, Hydrogel, and Exo groups. Two weeks after tooth extraction, mice maxillae were collected and fixed in 4% PFA.

In further experiments, NLRP3 inhibitor MCC950 (10 mg/kg, three times a week for one week, i.p.) or Raleukin (100 μg per mouse, local injection into the tooth socket) were injected into mice for further evaluation.

Patients

The present study involved five patients diagnosed with MRONJ.[1] However, a control group of five healthy donors who had undergone orthopedic surgeries was also included. Table S1 presents the clinical information. Clinical gingival samples were collected from patients who had undergone orthopedic or MRONJ surgeries at Peking University Hospital of Stomatology, and preserved at −80 °C for future examination.

All procedures were authorized by The Institutional Review Board of Peking University Hospital of Stomatology (Permit number: PKUSSIRB-202170184) and performed according to the principles of Declaration of Helsinki. Individuals enrolled in the study gave written informed consent.

MicroCT Analysis

The mice maxillae were scanned with a microCT scanner (60 kV, 2 mA, Inveon MM Gantry-STD 3121, Siemens, Germany). Three-dimensional images of maxillary tissues were reconstructed using Inveon Research Workplace (SIEMENS, Germany). Then, parameters of the bone microarchitecture of the tooth sockets, including BMD, BV/TV, and Tb.Th were determined. The data were analyzed with Image J.

Histology

The samples containing the extracted socket were dissected, fixed in 4% PFA, and decalcified in 10% ethylenediaminetetraacetic acid for 2 weeks at 37 °C. Next, the bone specimens were embedded in paraffin, and processed into 4-μm-thick slices for subsequent H&E and Masson staining following the instructions. Finally, the histological sections were observed and pictured with an Olympus microscope.

Immunochemistry Staining and Immunofluorescent Staining

For immunochemistry (IHC) staining, human and mice gingival sections were dewaxed with xylene and rehydrated with graded ethyl alcohol. Then, sections were incubated in 3% H_2O_2 for 20 min at RT, and treated with 10 mm sodium citrate buffer solution for 20 min at 95 °C. Next, the sections were cooled at RT and incubated with specific antibodies against TNF-α antibodies (ab1793, Abcam, Cambridge, UK), and IL-1β antibodies (ab9722, Abcam, Cambridge, UK) at 4 °C

overnight. Then, the sections were incubated with appropriate secondary antibodies for 20 min at RT. Finally, the sections were incubated with a DAB kit (P0203, Beyotime, China) and imaged using an Olympus microscope.

For immunofluorescent (IF) staining, human and mice gingival sections were also dewaxed with xylene and rehydrated with graded ethyl alcohol, and treated with 10 mm sodium citrate buffer solution for 20 min at 95 °C. Then, the sections were incubated with 0.1% Triton X-100 for 15 min, blocked in goat serum for 1 h at RT, and incubated with specific antibodies against iNOS (13120, CST, Boston, MA, USA), NLRP3 (15101, CST, Boston, MA, USA), GSDMD (39754, CST, Boston, MA, USA), CD68 (ab955, Abcam, Cambridge, UK) and F4/80 (ab6640, Abcam, Cambridge, UK) at 4 °C overnight and then incubated with TRITC-conjugated and FITC-conjugated secondary antibodies for 1 h RT. Next, nuclei were stained with DAPI and visualized with a fluorescence microscope. The positive area or cells were analyzed with Image J software.

Statistical Analysis

The data were analyzed using the GraphPad Prism 10 software and presented as the mean value-standard deviation. The unpaired two-tailed Student's *t*-test was used to determine the statistical significance of 2-group comparisons. The ANOVA analysis was used to determine the statistical significance among more than 2 groups. P values < 0.05 (*), <0.01 (**), <0.001 (***), <0.0001 (****) were considered statistically significant.

Results

ADSCs-Exo Prevents MRONJ by Accelerating Gingival Wound Healing in vivo

ADSCs showed spindle-shaped morphology (Figure S1A), alizarin red S-positive calcium deposits when cultured in the osteogenic medium, as well as oil-red O-positive lipid droplets when cultured in the adipogenic medium (Figure S1B and C). Moreover, ADSCs were positive for the MSCs-related markers (CD105, CD73, CD44, and CD90) but lack of hematopoietic markers (HLA-DR, CD19, CD45, CD11b, and CD34) (Figure S1D). In addition, Nanoparticle tracking analysis (NTA) and transmission electron microscopy (TEM) indicated that ADSCs-Exo were about 128 nm in diameter and displayed a round, cup-shaped morphology (Figure 1A and B) and positive expression for traditional Exo markers CD63 and CD9, as well as negative expression for calnexin (Figure 1C). The results of confocal scanning showed that PKH26-labelled Exo was uniformly distributed in the hydrogel and released slowly in vitro (Figure 1D and E).

MRONJ-like mouse model was constructed following a protocol described in our previous study.[20] Exo was then locally delivered into the tooth sockets to investigate whether Exo could promote tooth socket healing (Figure 1F). Two weeks later, the macrograph found that the zoledronate (Zol)-treated mice had an open alveolar socket, delayed oral mucosa healing, and exposed socket bone compared with the Ctrl group, while the Exo groups had intact covered mucosa (Figure 1G). MicroCT further suggested less bone formation in the tooth sockets of the Hydrogel and Zol groups versus the Exo and the Ctrl groups. In addition, decreased bone mineral density (BMD), bone volume fraction (BV/TV), and trabecular thickness (Tb.Th) were seen in the Hydrogel and Zol groups versus the Exo and Ctrl group (Figure 1H and I). Hematoxylin and eosin (H&E) staining suggested that the tooth sockets experienced a typical healing course, including full oral mucosal coverage, epithelial migration, and bone formation in the Ctrl group within two weeks. However, deficient epithelial lining, necrotic bones with empty lacunae, as well as inflammatory cells infiltration were found in the Hydrogel and Zol groups. Exo contributed to complete epithelial healing and bone formation of the tooth sockets (Figure 1J). Besides, Masson staining showed that the tooth sockets exhibited greater collagen fiber formation and deposit after Exo administration (Figure 1K). These data suggested that ADSCs-Exo prevented MRONJ by accelerating gingival wound healing in vivo.

Increased Pyroptosis and Inflammation Cytokines in MRONJ Patients

RNA sequence (RNA-seq) was then conducted on clinical gingival samples extracted from MRONJ patients and the healthy subjects. Principal component analysis showed a difference in MRONJ patients and healthy samples (Figure 2A). We identified 2295 differentially expressed genes (DEGs) in MRONJ patients, with 1597 up-regulated genes and 698 down-regulated genes by using the significance threshold of $|\log2 \text{ fold change}| \geq 1$ and q value ≤ 0.05 as criteria (Figure 2B). The up-

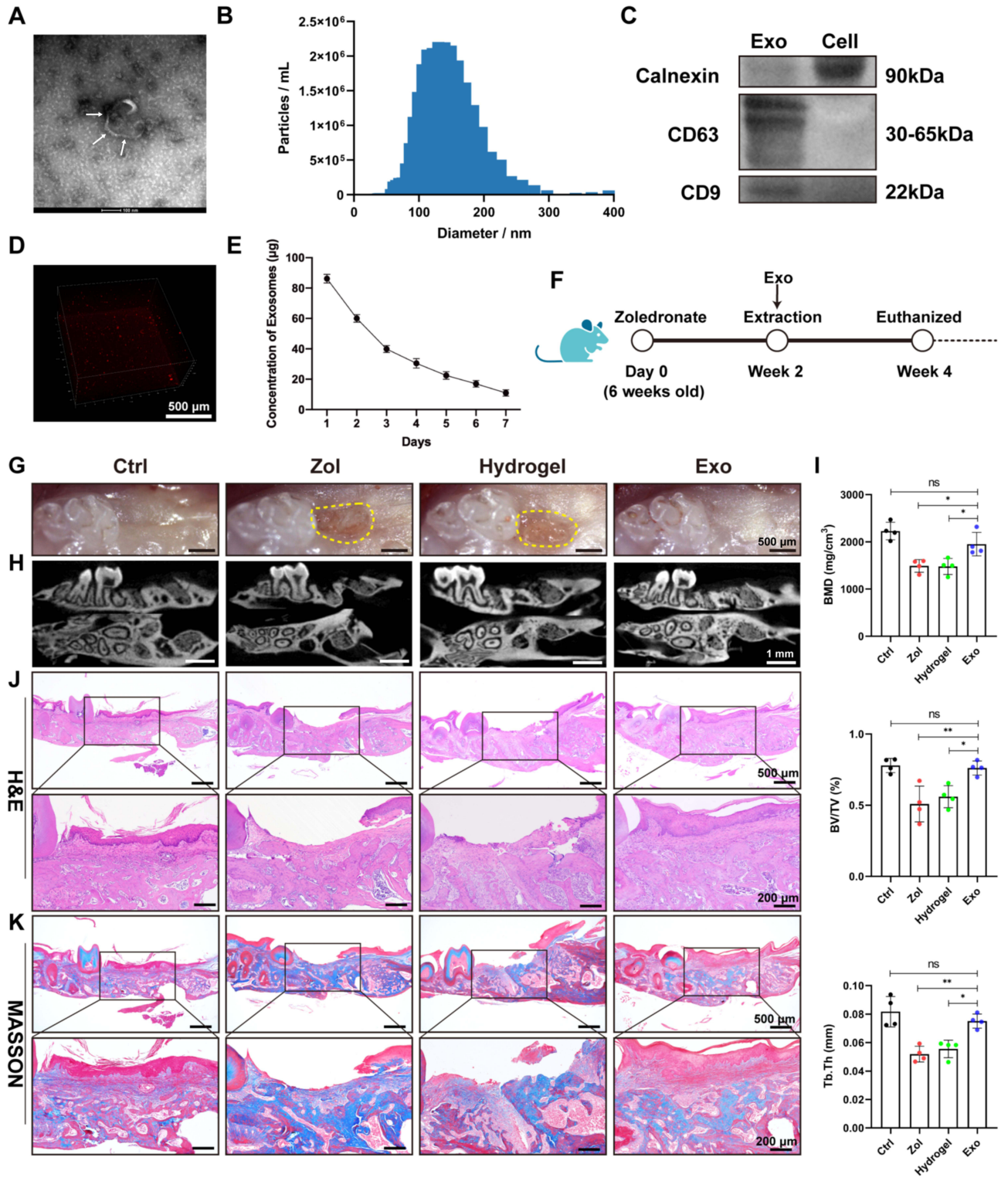

Figure 1 ADSCs-Exo promotes tooth socket wound healing in MRONJ-like mice. **(A)** TEM observation of Exo morphology. White arrowheads indicate Exo. Scale bar = 100 nm. **(B)** NTA analysis of particle size distribution of Exo. **(C)** Western blot analysis of the specific markers of Exo and ADSCs. **(D)** Confocal microscopy images of PKH26-labelled Exo distributed in the hydrogel. Scale bar = 500 μm. **(E)** BCA assay of the release rate of Exo in the hydrogel *in vitro*. **(F)** Experimental protocol of how to use Exo to prevent MRONJ. n=5 per group. **(G)** A macrograph of tooth sockets. Yellow dot circles mark the delayed oral mucosa closure area. Scale bar = 500 μm. **(H)** MicroCT scan of tooth sockets. Scale bar = 1 mm. **(I)** Analysis of BMD, BV/TV, and Tb.Th of tooth sockets. **(J)** H&E staining of tooth sockets. Black square indicates the magnified areas. Scale bar = 500 μm (top row) and 200 μm (bottom row). **(K)** Masson staining of tooth extraction sockets. Black square indicates the magnified areas. Scale bar = 500 μm (top row) and 200 μm (bottom row). Data in this figure, mean ± SD, ns = not significant, *p<0.05, **p<0.01.

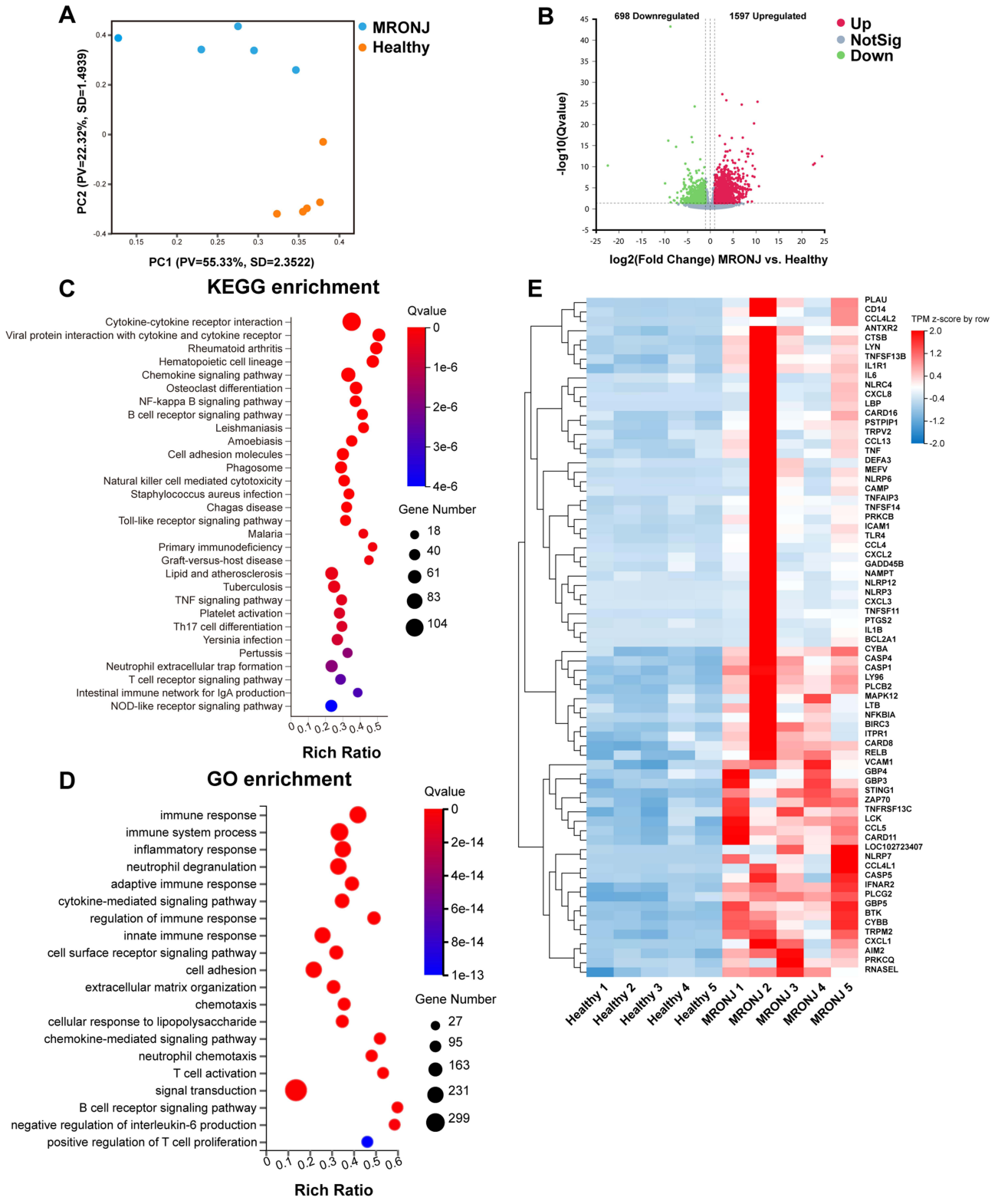

Figure 2 RNA-Transcriptome sequencing of clinical gingival samples from MRONJ patients and healthy subjects. **(A)** Principal component analysis of the two groups. **(B)** Volcano plot showing up-regulated 1597 genes and down-regulated 698 genes in the two groups. **(C)** KEGG enrichment analyses of the 1597 up-regulated genes in MRONJ patients. **(D)** GO enrichment analyses of the 1597 up-regulated genes in MRONJ patients. **(E)** Heatmap analysis of genes in the NOD/NF-κB signaling pathway.

https://doi.org/10.2147/IJN.S482849 DovePress

regulated DEGs were chosen for KEGG and GO enrichment analyses, which were related to pyroptosis and inflammation pathways, for example, NF-κB signaling pathway, TNF signaling pathway, NOD-like receptor signaling pathway, immune response, and inflammatory response (Figure 2C and D). The heatmap showed the expression level of 72 pyroptosis-related DEGs in the NOD/NF-κB signaling pathway (Figure 2E). Protein-protein interaction (PPI) analysis assessed the interaction among 72 pyroptosis-related DEGs and suggested that *IL-1β, BCL2A1, TNF-α, CXCL8, IL-6, LBP, NLRP3*, and *CASP1* are overlapping hub genes (Figure S2). Furthermore, Western blot results confirmed that inflammasome-related proteins, like NLR family pyrin domain containing 3 (NLRP3) and gasdermin D (GSDMD), and cleaved-caspase-1, were increased in gingival tissues collected from MRONJ patients (Figure 3A and B). The heatmap indicated higher expression of M1 macrophage-related genes in MRONJ patients (Figure 3C).

ADSCs-Exo Prevents MRONJ by Regulating Macrophage M1 Polarization and Pyroptosis in vivo

Next, we assessed the impact of ADSCs-Exo on regulating macrophage M1 activation and pyroptosis in MRONJ mice. Our results showed Zol significantly increased gingival tissue M1 macrophages (CD68+iNOS+ cells) in MRONJ patients and M1 macrophages (F4/80+iNOS+ cells) in mice samples (Figure 3D–I). Also, pyroptosis-related proteins, NLRP3 and GSDMD, were both highly expressed in the gingiva in MRONJ patients and Zol-treated mice. However, Exo administration reduced the NLRP3 and GSDMD expression (Figure 3E–K). Meanwhile, the gingival tissue showed increased expression of pro-inflammatory factors (IL-1β and TNF-α), indicating that the macrophage inflammation-related activity accompanied the gingival wound and inflammatory response induced by Zol. On the contrary, Exo administration could decrease M1 macrophage activation and alleviate tissue inflammation (Figure 3G–M). These results suggested that ADSCs-Exo inhibited Zol-induced macrophage M1 polarization and pyroptosis in vivo.

NLRP3 Inhibitors MCC950 Rescues the Lesions of MRONJ by Inhibiting Macrophage Pyroptosis

To investigate the role of pyroptosis in MRONJ, we administered NLRP3 inhibitor MCC950 (inhibitor of pyroptosis) to the Zol-treated mice (Figure 4A). The clinical examination showed intact oral mucosa coverage without bone exposure in the MCC950 group versus the Zol-treated mice (Figure 4B). MicroCT analysis further showed that the MCC950 group had more new bone regeneration, with elevated BMD, BV/TV, and Tb.Th (Figure 4C and D). H&E and Masson staining showed that the tooth sockets in the MCC950 group had complete epithelial lining, collagen synthesis, and new bone formation versus the Zol group (Figure 4E and F). Furthermore, histological staining showed fewer local M1 macrophages and a decreased pyroptosis response, with less expression of GSDMD and NLRP3 in the gingiva tissue of MCC950 group (Figure 4G–L). Besides, IL-1β and TNF-α expression in the gingiva wound tissue were significantly decreased in the MCC950 group versus the Zol group (Figure 4J-L). These data suggested the role of macrophage pyroptosis in the development of MRONJ.

ADSCs-Exo and MCC950 Inhibit Macrophage M1 Polarization and Pyroptosis by NF-κB/NLRP3/IL-1β Axis in vitro

Next, bone marrow-derived macrophages (BMDMs) were cultured with PKH26-labeled Exo in vitro to verify animal data. BMDMs could internalize PKH26-labeled Exo and increase the content over time at 6 h, 12 h, and 24 h (Figure 5A). According to the CCK-8 assay results, 25 μM Zol was used to minimize the adverse effects on cell viability (Figure 5B). BMDMs were pre-treated with Zol, Exo, and MCC950 for 24 h, then exposed to lipopolysaccharide (LPS) for 4 h, which could activate macrophages to M1 phenotype. Next, nigericin was used to activate the pyroptosis in BMDMs for 1 hour after LPS stimulation. Flow cytometry revealed that Zol significantly raised the percentage of M1 macrophages (CD86+CD206- cells) from 42.2% to 70.0%, while Exo and MCC950 decreased M1 macrophages from 70% to 46.5% and 50.5%, respectively (Figure 5C and D). This is consistent with the result obtained by cell IF staining. After Zol treatment, BMDMs expressed higher iNOS expression, a marker of M1 macrophage, while Exo and MCC950 could significantly decrease iNOS expression (Figure 5E and F). Furthermore, Zol increased the

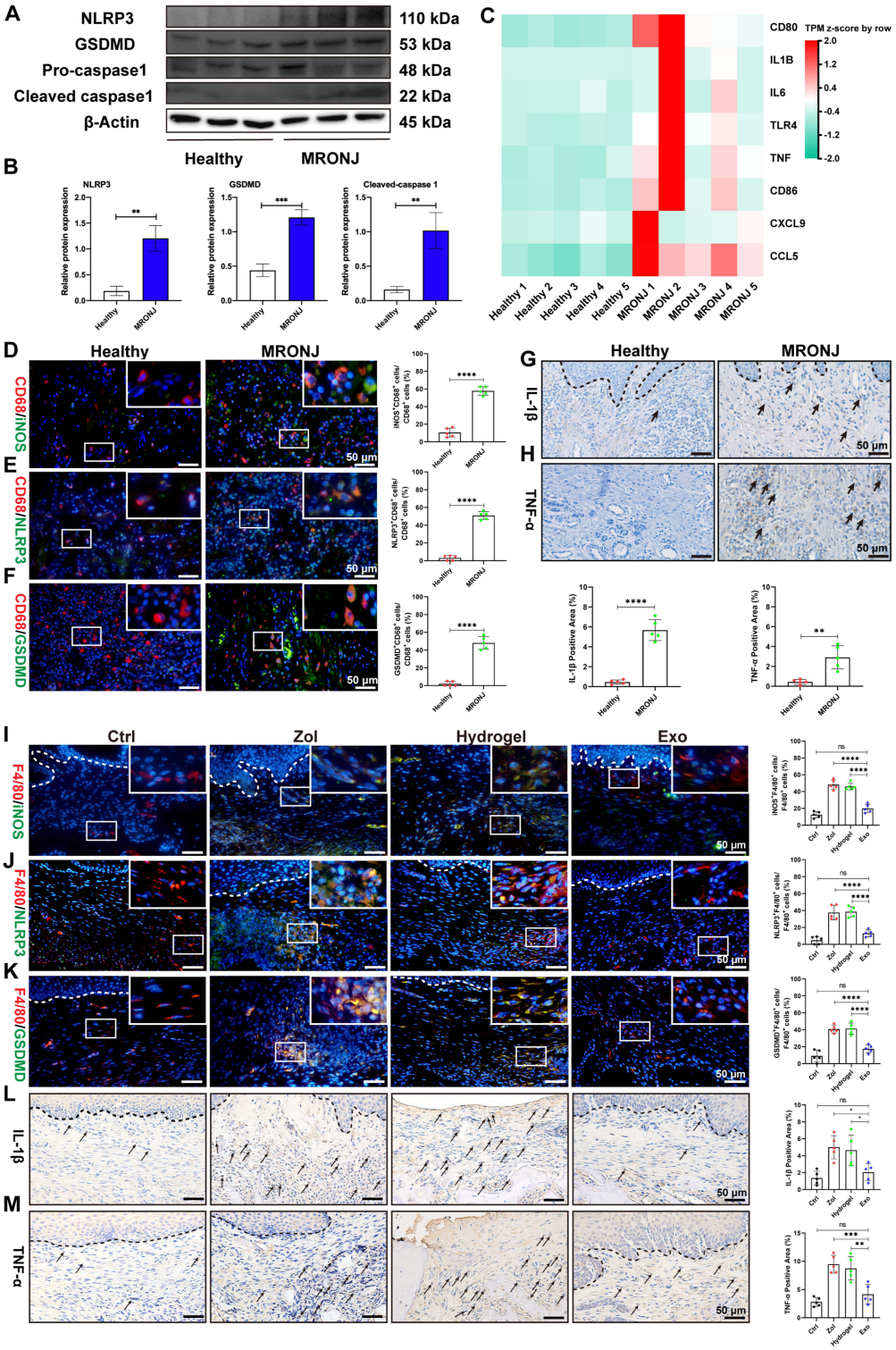

Figure 3 ADSCs-Exo inhibits M1 macrophage activation and pyroptosis induced by Zol. **(A** and **B)** NLRP3, GSDMD, and cleaved-caspase-1 levels by Western blot in MRONJ patients. **(C)** Heatmap analysis of M1 macrophage-related genes in MRONJ patients. **(D)** IF staining for CD68 and iNOS in MRONJ patients. White square indicates the magnified areas. Scale bar = 50 μm. **(E)** IF staining for CD68 and NLRP3 in MRONJ patients. Scale bar = 50 μm. **(F)** IF staining for CD68 and GSDMD in MRONJ patients. Scale bar = 50 μm. **(G)** IHC staining for IL-1β in MRONJ patients. The black dashed lines represent the demarcation between epithelial and connective tissue. Black arrowheads indicate the IL-1β-positive area. Scale bar = 50 μm. **(H)** IHC staining for TNF-α in MRONJ patients. Black arrowheads indicate the TNF-α-positive area. Scale bar = 50 μm. **(I)** IF staining for F4/80 and iNOS in mouse samples. The white dashed lines represent the demarcation between epithelial and connective tissue. Scale bar = 50 μm. **(J)** IF staining for F4/80 and NLRP3 in mouse samples. Scale bar = 50 μm. **(K)** IF staining for F4/80 and GSDMD in mouse samples. Scale bar = 50 μm. **(L)** IHC staining for IL-1β in mouse samples. Scale bar = 50 μm. **(M)** IHC staining for TNF-α in mouse samples. Scale bar = 50 μm. Data in this figure, mean ± SD, ns = not significant, *p<0.05, **p<0.01, ***p<0.001, ****p<0.0001.

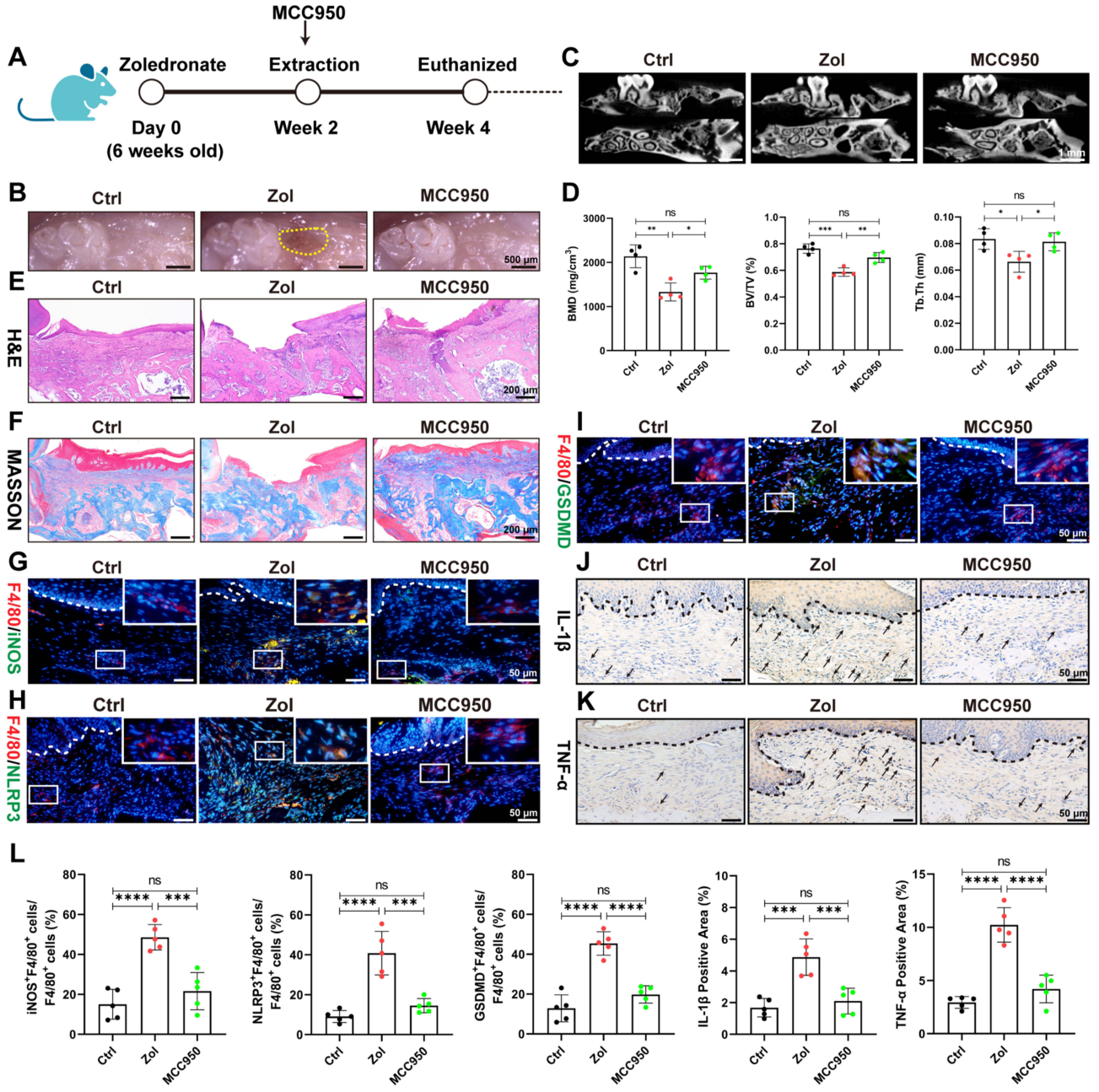

Figure 4 NLRP3 inhibitor MCC950 prevents MRONJ by inhibiting M1 macrophage activation and pyroptosis in vivo. **(A–F)** Amelioration of MRONJ-like lesion formation by NLRP3 inhibitor MCC950 intraperitoneal. n=5 per group. **(G)** IF staining for F4/80 and iNOS. White square indicates the magnified areas. Scale bar = 50 μm. **(H)** IF staining for F4/80 and NLRP3. Scale bar = 50 μm. **(I)** IF staining for F4/80 and GSDMD. Scale bar = 50 μm. **(J)** IHC staining for IL-1β. Black arrowheads indicate the IL-1β-positive area. Scale bar = 50 μm. **(K)** IHC staining for TNF-α. Scale bar = 50 μm. **(L)** The quantitative analysis of the numbers of F4/80+iNOS+ M1 macrophages, F4/80+NLRP3+ macrophages, F4/80+GSDMD+ macrophages, IL-1β-positive area, TNF-α-positive area by ImageJ software. Data in this figure, mean ± SD, ns = not significant, *p<0.05, **p<0.01, ***p<0.001, ****p<0.0001.

inflammasome-related proteins, like NLRP3, GSDMD, and cleaved-caspase-1, in BMDMs in vitro. Such enhanced effects were significantly counteracted by the Exo or MCC950 administration (Figure 5G and H). Furthermore, IF staining showed an increase in NLRP3 and GSDMD expression in Zol-affected BMDMs, which was significantly reduced in BMDMs after Exo and MCC950 administration (Figure 6A and B).

Given that the NLRP3 inflammasome signal is a possible target of the NF-κB signaling pathway, we assessed the protein levels of NF-κB family members, including the degradation level of the nuclear factor of kappa light polypeptide gene enhancer in B-cell inhibitor α (IκBα) and transcription factor P65 phosphorylation (p-P65) level in the BMDMs. Zol

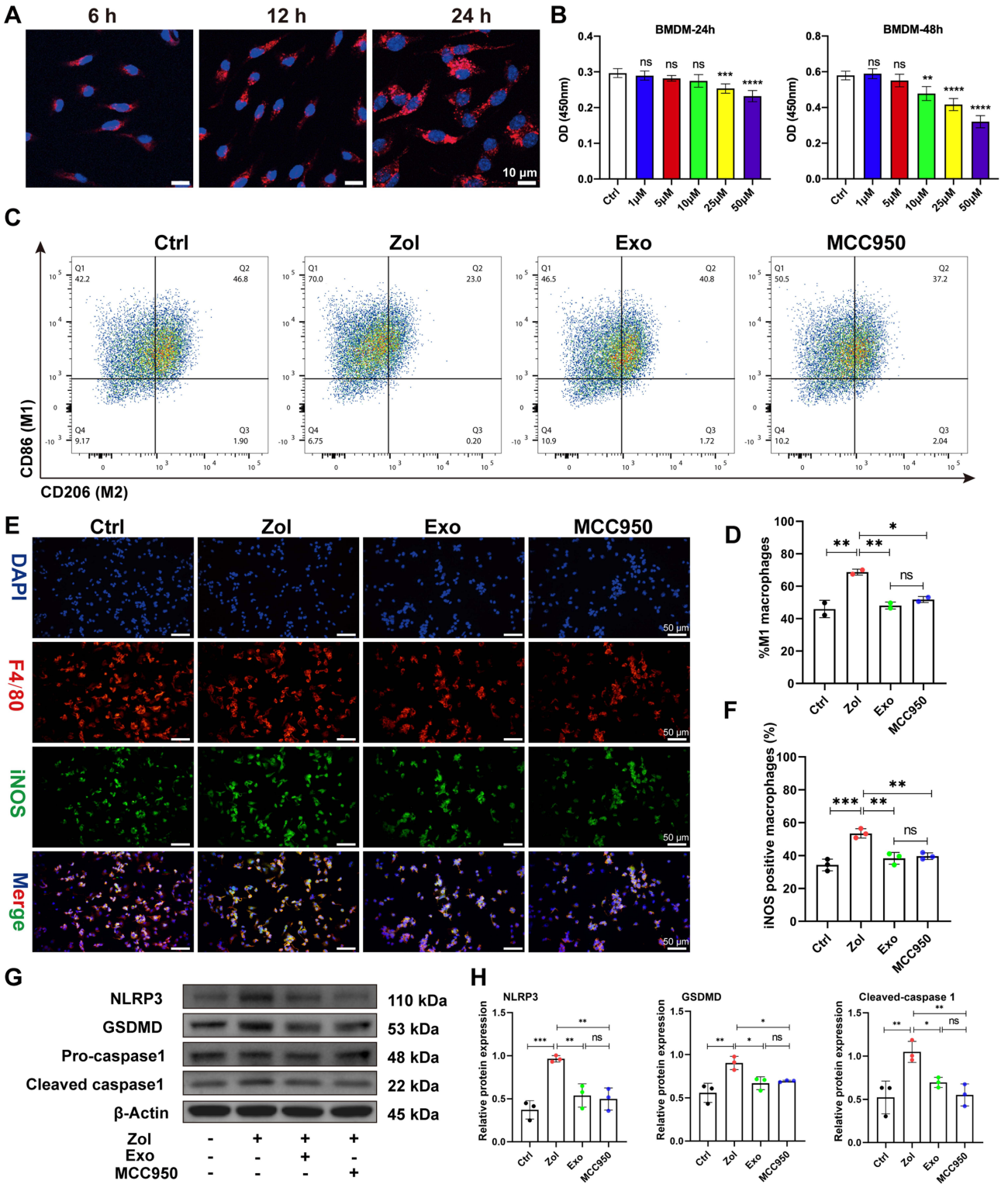

Figure 5 ADSCs-Exo and MCC950 inhibit M1 macrophage activation and pyroptosis induced by Zol. **(A)** Confocal microscopy images of PKH26-labelled Exo internalized by BMDMs. Scale bar = 10 μm. **(B)** CCK8 assessment of the impact of the different doses of Zol on BMDMs proliferation. **(C** and **D)** Flow cytometry analysis of CD86 and CD206 expression on BMDMs. **(E** and **F)** IF staining for iNOS and F4/80 in BMDMs. Scale bar = 50 μm. **(G** and **H)** NLRP3, GSDMD, and cleaved-caspase-1 levels by Western blot in BMDMs. Data in this figure, mean ± SD, ns = not significant, *p<0.05, **p<0.01, ***p<0.001, ****p<0.0001.

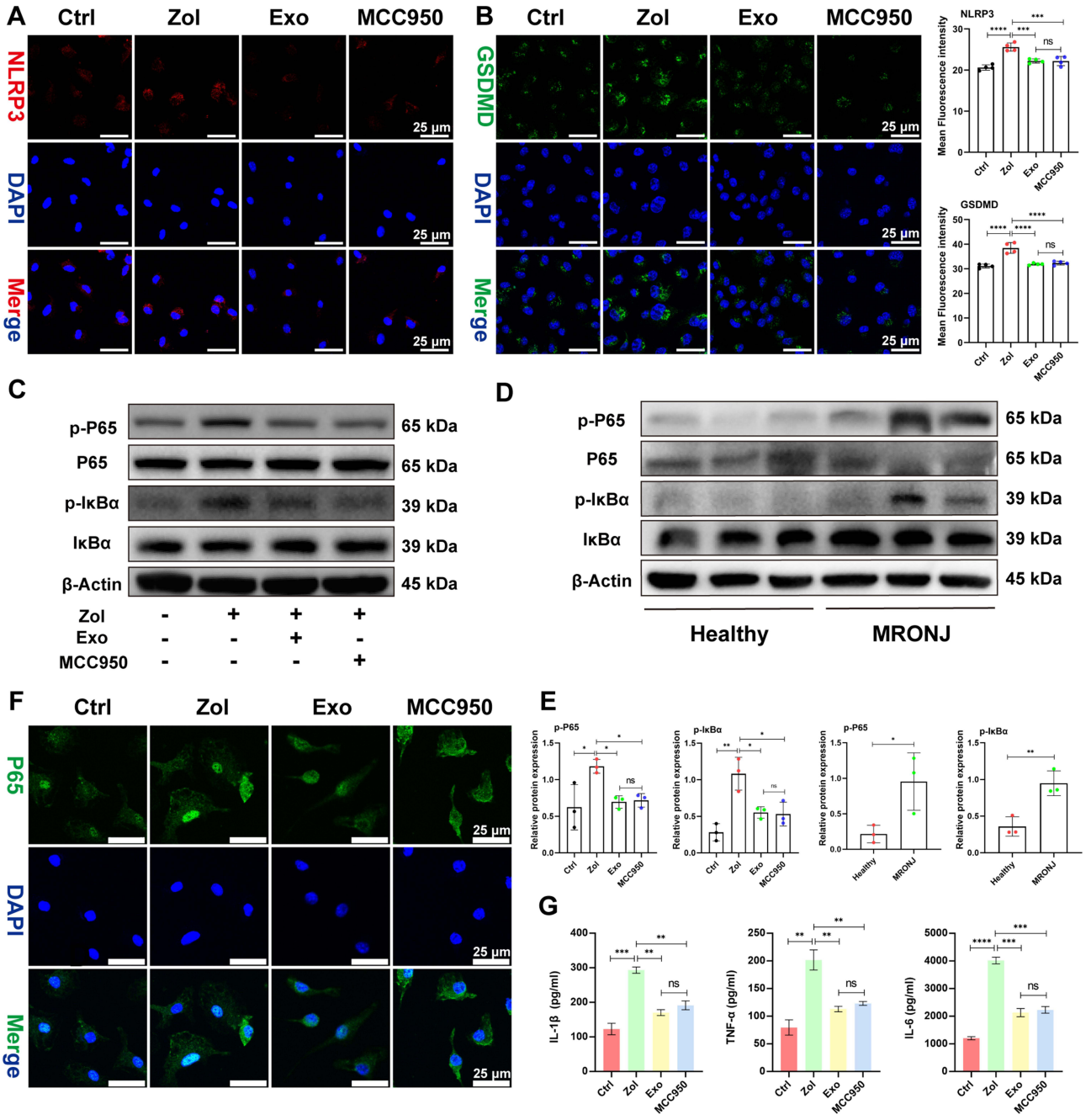

Figure 6 ADSCs-Exo and MCC950 inhibit pyroptosis by NF-κB signaling pathway in vitro. **(A)** IF staining for NLRP3 in BMDMs. Scale bar = 25 μm. **(B)** IF staining for GSDMD in BMDMs. Scale bar = 25 μm. **(C–E)** P65, p-P65, IκBα, and p-IκBα levels by Western blot in BMDMs and MRONJ patients. **(F)** IF staining for P65 in BMDMs. Scale bar = 25 μm. **(G)** IL-1β, TNF-α, and IL-6 levels by ELISA. Data in this figure, mean ± SD, ns = not significant, *p<0.05, **p<0.01, ***p<0.001, ****p<0.0001.

enhanced NF-κB activation, as evidenced by an increase in the proportion of p-P65 and p-IκBα levels in BMDMs and MRONJ patients, while Exo and MCC950 administration greatly attenuated phosphorylation of IκBα and p65 (Figure 6C–E). Furthermore, IF staining showed that p65 was located more in the nucleus after treatment with Zol, but Exo and MCC950 inhibited phosphorylation and transfer of p65 into the nucleus (Figure 6F). For further validation, the release of pro-inflammatory mediators, TNF-α, IL-1β, and IL-6 were up-regulated in Zol-exposed BMDMs as assessed by ELISA, which could be inhibited by Exo and MCC950 treatment (Figure 6G). These findings supported that Exo and MCC950 dramatically suppressed NF-κB signaling activation and subsequent pyroptosis in BMDMs.

IL-1RA Derived from ADSCs-Exo is the Key Factor in Preventing MRONJ

Interleukin-1 receptor antagonist (IL-1RA) derived from gingival mesenchymal stromal cells plays a key role in promoting gingival wound healing.[37] Also, IL-1RA is a natural inhibitor of IL-1β, which could effectively inhibit the inflammatory response.[38] Therefore, we performed IF staining and found that Zol reduced IL-1RA expression in the gingiva tissue of both MRONJ patients and Zol-treated mice versus the Ctrl group. However, ADSCs-Exo treatment significantly improved IL-1RA expression (Figure 7A and B). Then, IF staining confirmed that ADSCs contained IL-1RA (Figure 7C), and Western blot results indicated that ADSCs-Exo was rich in IL-1RA (Figure 7D). To further verify the role of IL-1RA in the prevention of MRONJ, Raleukin, a recombinant IL-1RA, was used in the subsequent experiments. Raleukin effectively promoted wound healing and bone regeneration of the tooth sockets and reduced macrophage pyroptosis and inflammatory response in the gingiva tissue in vivo (Figure 7E–J and 8A–G). Furthermore, Raleukin reduced Zol-induced BMDMs pyroptosis and inflammatory cytokines release by inhibiting NF-κB/NLRP3/IL-1β axis in vitro (Figure 8H–M and S3). These results confirmed that IL-1RA derived from ADSCs-Exo might be crucial in preventing MRONJ.

Discussion

Exosomes exert crucial functions in intercellular communications by delivering multiple bioactive molecules between cells.[16,39,40] For example, ADSCs-Exo could transfer mitochondria components to alveolar macrophages, improving homeostasis and reducing lung inflammatory conditions.[41] Also, another study found that ADSCs-Exo can reduce inflammation response and oxidative stress by regulating the function of macrophages in sepsis.[42] Consistently, we found that Exo can inhibit macrophage M1 polarization and gingival inflammation, accelerate gingiva wound closure, and increase bone mass in the tooth extraction sockets. In vitro studies further suggested that Exo can reverse macrophage M1 activation and pyroptosis induced by Zol. These findings suggest that macrophage may be the crucial target in ADSCs-Exo meditated gingival healing and prevention of MRONJ.

Pyroptosis is an inflammatory cell death that occurs in macrophages upon pathogen infection. It is accompanied by cell swelling, membrane rupture, and the release of cellular contents, which causes the secretion of pro-inflammatory cytokines, such as IL-1β, IL-18, TNF-α, and IL-6.[43–45] Mechanistically, pathogen-associated molecular patterns (PAMPs) and damage-associated molecular patterns induce pyroptosis by pattern recognition receptors, like Toll-like receptors (TLRs) and NOD-like receptors.[46] Although pyroptosis is vital for the host immune defense against pathogenic infection in normal physiology, excessive and uncontrolled pyroptosis can result in extensive and chronic inflammatory responses.[47,48] Previous studies have demonstrated that macrophage pyroptosis could release IL-1β and exert pyroptosis-related cytotoxic effects in delayed chronic wounds, which could be reversed by macrophage pyroptosis and inflammatory response amelioration.[29] NF-κB family members have a crucial impact on inflammatory cytokine release and can affect M1 macrophage polarization and NLRP3 inflammasome.[49–51] TLRs can recognize PAMPs and activate the NF-κB signaling pathway, leading the IκBα/NF-κB complex to be phosphorylated and dissociated.[52] IκBα degradation and P65 nuclear translocation initiate target gene transcription, like NLRP3, promoting M1 polarization and pyroptosis, ultimately releasing numerous mature inflammatory mediators.[53,54] In addition, NLRP3 activation increases the secretion of caspase-1, accelerates the disruption of GSDMD (effector of pyroptosis) and IL-1β, and causes pyroptosis and inflammatory response.[55] Zol can activate TLR4 signaling, induce the NF-κB nuclear translocation, and produce pro-inflammatory cytokines in macrophages.[56] RNA-seq results demonstrated the pyroptosis and inflammatory processes were up-regulated in MRONJ patients, such as NF-κB signaling pathway and NOD-like receptor signaling pathway. Heatmap results further confirmed that Zol could significantly up-regulate the expression of M1 macrophage related-markers (CD80, IL-1β, IL-6, TLR4, TNF-α, CD86, CXCL9, CCL5), and expression of NLRP3 complexes (NLRP3 and CASP1). These results demonstrate that macrophage M1 polarization and pyroptosis might have an essential function in the pathogenesis of MRONJ.

Exosomes affect macrophage M1 polarization and pyroptosis in many diseases. For example, Exo can reduce M1 macrophage numbers, inflammation-induced pyroptosis, and harmful cardiac remodeling[57] or attenuate DSS-induced colitis.[26] Our study found that more M1 macrophages and pro-inflammatory cytokines existed in the gingiva tissue

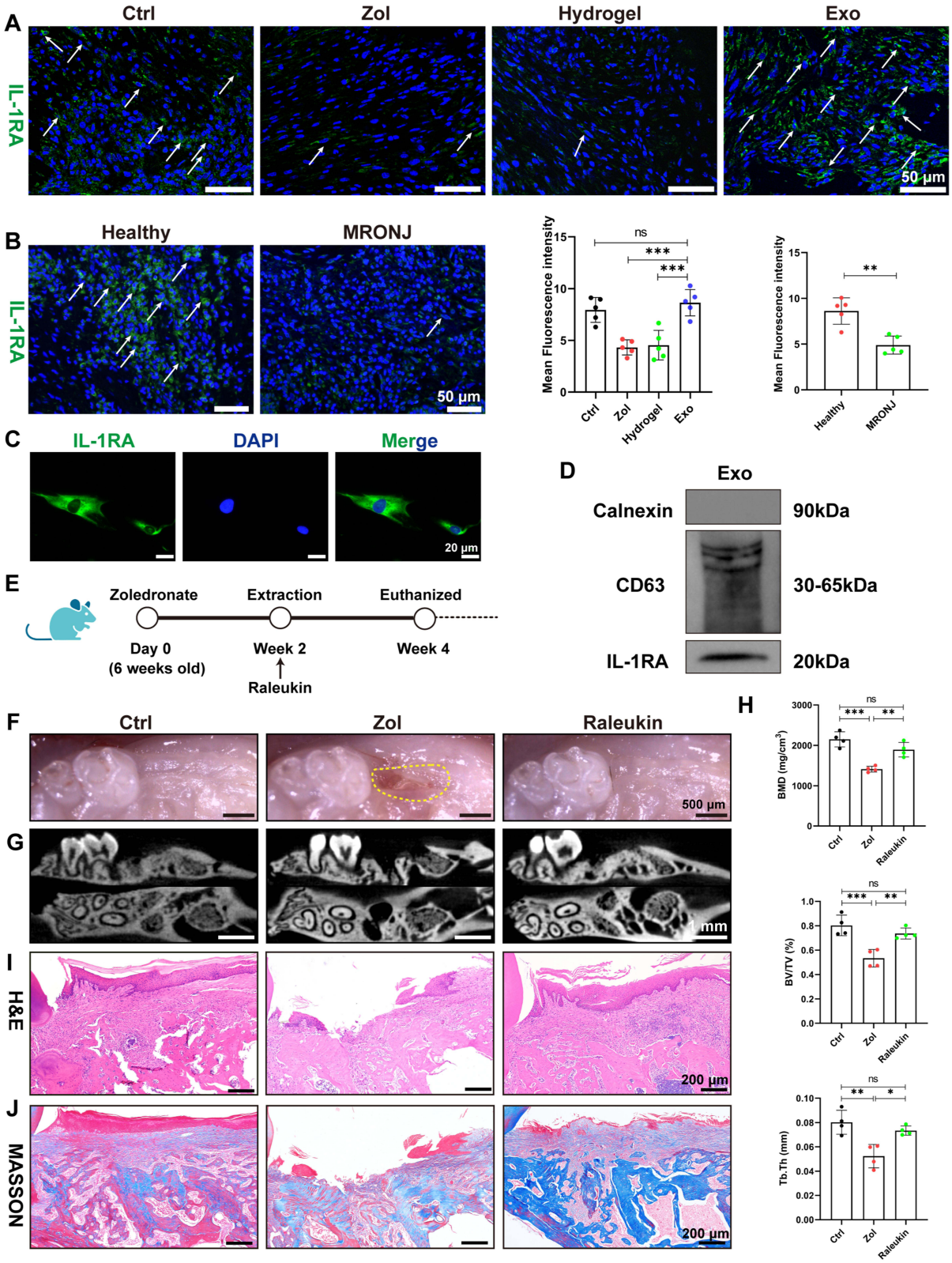

Figure 7 Raleukin promotes tooth socket wound healing in MRONJ-like mice. **(A)** IF staining for IL-1RA in mouse samples. White arrowheads indicate the IL-1RA-positive area. Scale bar = 50 μm. **(B)** IF staining for IL-1RA in MRONJ patients. Scale bar = 50 μm. **(C)** IF staining of IL-1RA in ADSCs. Scale bar = 20 μm. **(D)** Western blot analysis of the expression of IL-1RA in Exo. **(E–J)** Amelioration of MRONJ-like lesion formation by Raleukin. n=5 per group. Data in this figure, mean ± SD, ns = not significant, *p<0.05, **p<0.01, ***p<0.001.

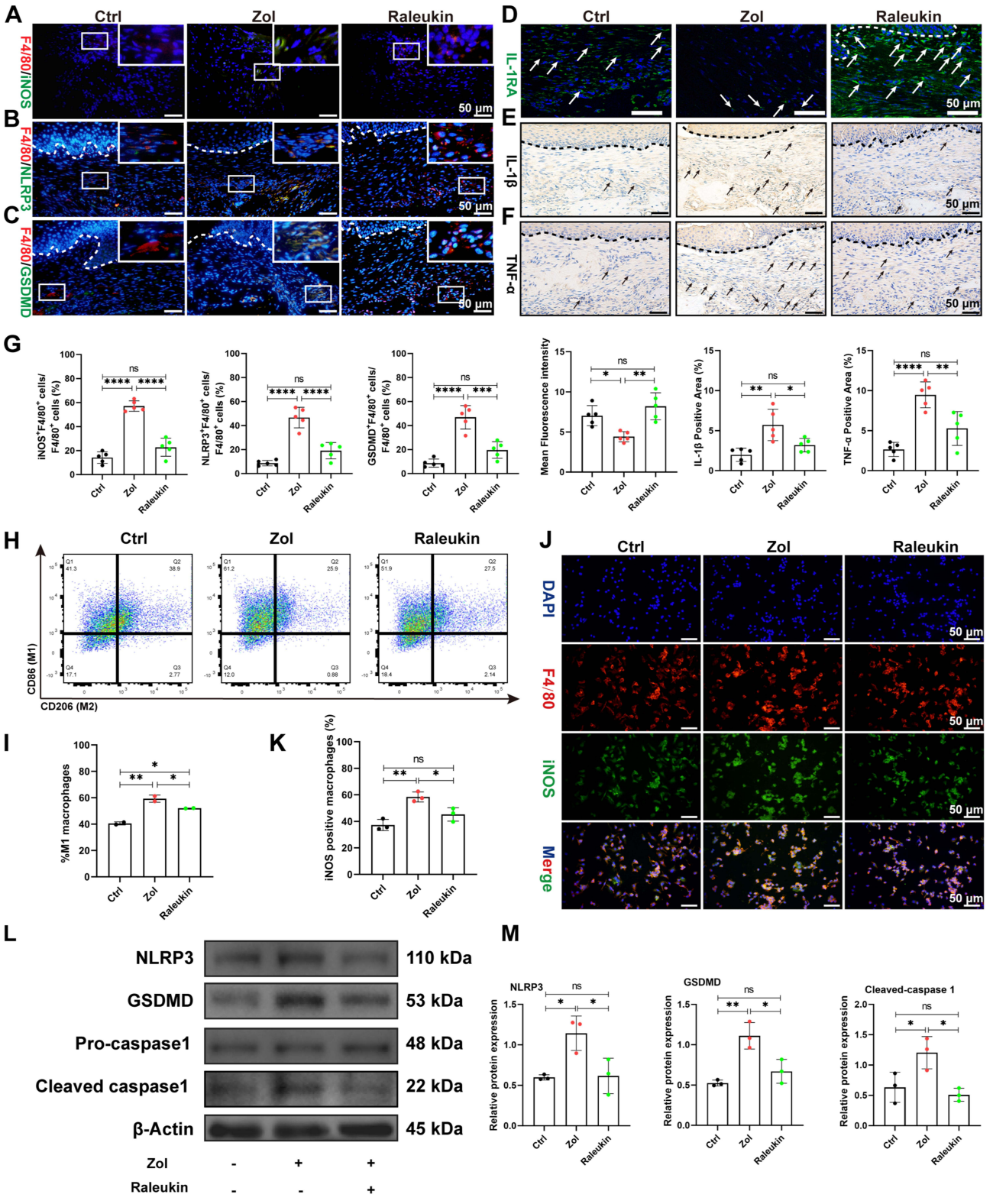

Figure 8 Raleukin inhibits M1 macrophage activation and pyroptosis induced by Zol. **(A)** IF staining for F4/80 and iNOS. White square indicates the magnified areas. Scale bar = 50 μm. **(B)** IF staining for F4/80 and NLRP3. Scale bar = 50 μm. **(C)** IF staining for F4/80 and GSDMD. Scale bar = 50 μm. **(D)** IF staining for IL-1RA. White arrowheads indicate the IL-1RA-positive area. Scale bar = 50 μm. **(E)** IHC staining for IL-1β in MRONJ patients. Black arrowheads indicate the IL-1β-positive area. Scale bar = 50 μm. **(F)** IHC staining for TNF-α in MRONJ patients. Scale bar = 50 μm. **(G)** The quantitative analysis of the numbers of F4/80+iNOS+ M1 macrophages, F4/80+NLRP3 + macrophages, F4/80+GSDMD+ macrophages, IL-1RA-positive area, IL-1β-positive area, TNF-α-positive area by ImageJ software. **(H-I)** Flow cytometry analysis of CD86 and CD206 expression on BMDMs. **(J-K)** IF staining for iNOS and F4/80 in BMDMs. Scale bar = 50 μm. **(L** and **M)** NLRP3, GSDMD, and cleaved-caspase-1 levels by Western blot in BMDMs. Data in this figure, mean ± SD, ns = not significant, *p<0.05, **p<0.01, ***p<0.001, ****p<0.0001.

during tooth sockets wound healing in vivo, while Exo could reduce excessive M1 macrophage infiltration and IL-1β, TNF-α expression during the wound healing process. Besides, GSDMD and NLRP3 expression significantly increased in the gingiva tissue, which could be alleviated by Exo. Exo could also attenuate Zol-effected macrophage shift into M1 phenotype and pyroptosis and decrease pro-inflammatory cytokines, like IL-1β, IL-6, and TNF-α release in vitro. Furthermore, MCC950, an NLRP3 inhibitor, could effectively alleviate M1 macrophage activation and pyroptosis and rescue the development of MRONJ *in* vivo and in vitro. Our results indicate that ADSCs-Exo could target the NF-κB/NLRP3/IL-1β axis in macrophages to prevent MRONJ.

NLRP3 inflammasome activation and caspase-1 cleavage lead to the maturation and secretion of IL-1β, which is considered a key cytokine in amplifying the inflammatory response. IL-1RA is a natural inhibitor of IL-1β, which can effectively block IL-1β-driven inflammatory signals and regulate immune status.[38] IL-1RA can effectively inhibit the activity of inflammasome.[58] For example, recombinant IL-1RA could inhibit NLRP3 inflammasome activation and reduce liver inflammation by reducing intracellular ROS levels.[59] IL-1RA knockout mice may develop severe inflammatory responses related to infection, but exogenous supplementation of Raleukin can reduce excessive inflammatory responses and tissue damage.[60] In our study, the exploration of the mechanism by which ADSCs-Exo inhibits NLRP3 inflammasome activation revealed that IL-1RA plays a key role in preventing MRONJ (Figure 9). We found that ADSCs-Exo was rich in IL-1RA. Raleukin, a recombinant IL-1RA, effectively alleviated NLRP3 inflammasome activation and pyroptosis and prevented MRONJ in vivo. Additionally, Raleukin reduced Macrophage M1 polarization and pyroptosis in BMDMs by blocking NF-κB/NLRP3/IL-1β axis in vitro.

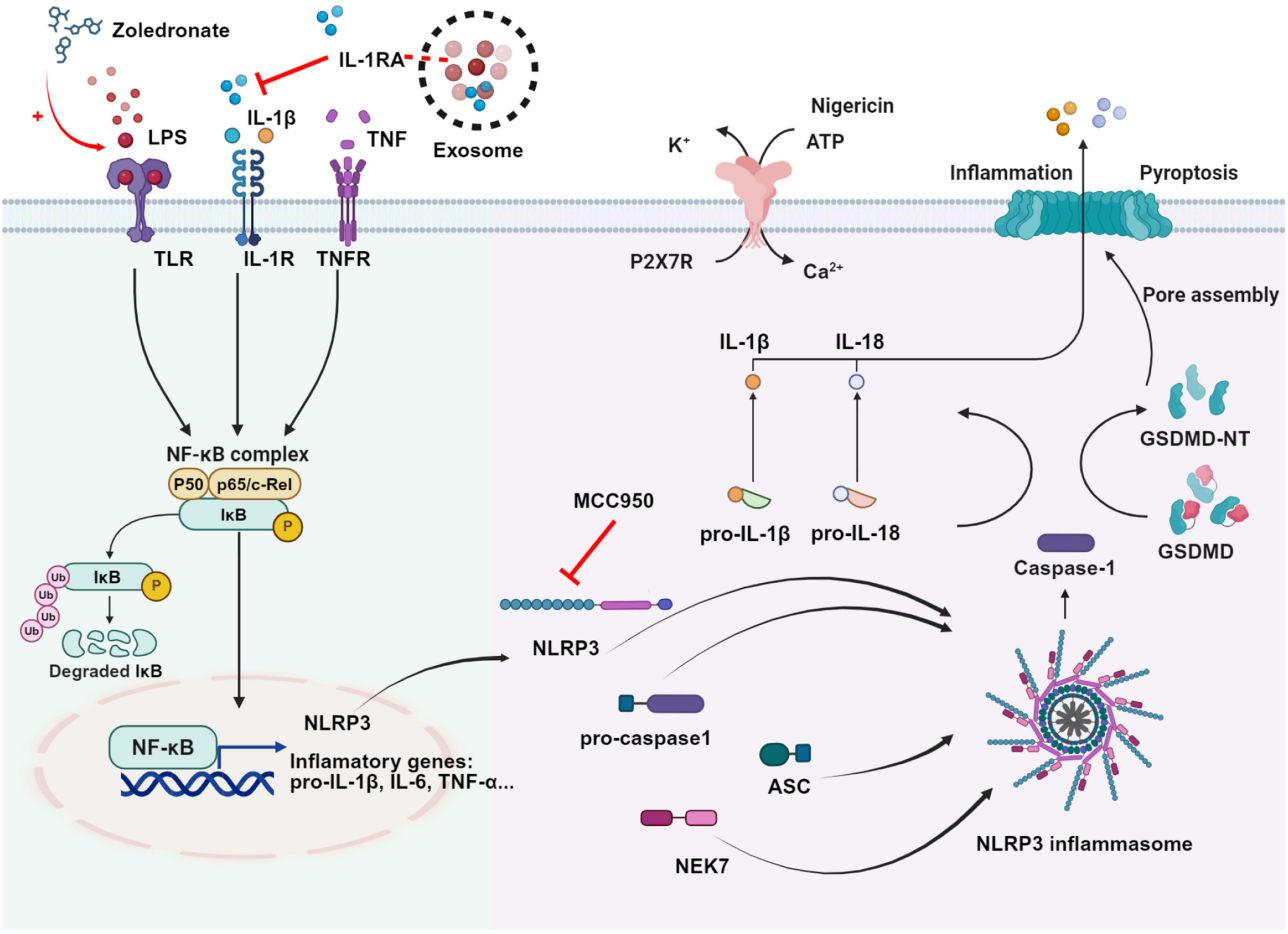

Figure 9 The mechanism of how ADSCs-Exo prevents the onset of MRONJ. Zol promotes macrophage M1 polarization and pyroptosis, causing the release of IL-1β. IL-1β can stimulate the IL-1R on the cell surface to form a positive feedback effect, cascading pyroptosis and inflammatory response. Excessive pyroptosis and the release of inflammatory factors delay the healing of tooth extraction sockets. IL-1RA derived from ADSCs-Exo can competitively bind to the IL-1R on the cell membrane surface and block the effect of IL-1β. IL-1RA inhibits the macrophage M1 polarization and pyroptosis by inhibiting the NF-κB/NLRP3/IL-1β axis, reducing the release of proinflammatory cytokines such as IL-1β and TNF-a in the tooth extraction sockets, thus promoting wound healing and preventing the occurrence of MRONJ.

However, our present study has limitations. The results only revealed the role of macrophages in the prevention of MRONJ by ADSCs-Exo, but did not explore the regulatory effects of ADSCs-Exo on other cells, like osteoblasts, osteoclasts, endothelial cells, and epithelial cells. In future studies, more research is needed to investigate the possible interactions between ADSCs-Exo and other cells.

Conclusion

In conclusion, our study indicated that macrophage pyroptosis is increased in MRONJ wound healing, which might cause the release of inflammatory cytokines and delay wound healing. IL-1RA derived from ADSCs-Exo attenuated macrophage M1 polarization and pyroptosis, reduced tissue inflammation by blocking NF-κB/NLRP3/IL-1β axis, and promoted primary gingival wound closure to prevent MRONJ. Consequently, our research sheds light on the pathophysiology of MRONJ and might offer an appropriate strategy for preventing MRONJ.

Abbreviations

ADSCs, adipose-derived mesenchymal stromal cells; ADSCs-Exo, exosomes derived from ADSCs; BMD, bone mineral density; BMDMs, bone marrow derived macrophages; BPs, bisphosphonates; BV/TV, bone volume/total volume; CCK8, cell counting kit-8; DAPI, 4′, 6-diamidino-2-phenylindole; DEGs, differentially expressed genes; ELISA, enzyme-linked immunosorbent assay; Exo, Exosomes; GSDMD, gasdermin D; H&E, hematoxylin and eosin; IF, immunofluorescent; IHC, immunochemistry; IκBα, nuclear factor of kappa light polypeptide gene enhancer in B-cell inhibitor α; IL-1RA, interleukin-1 receptor antagonist; IL-1β, interleukin-1β; LPS, lipopolysaccharide; MRONJ, medication-related osteonecrosis of the jaw; MicroCT, micro computed tomography; NLRP3, NLR family pyrin domain containing 3; NTA, nanoparticle tracking analysis; PAMPs, pathogen-associated molecular patterns; PBS, phosphate buffer saline; PFA, paraformaldehyde; PPI, protein-protein interaction; RNA-seq, RNA sequence; RPMI, Roswell Park Memorial Institute; RT, room temperature; Tb.Th, trabecular thickness; TEM, transmission electron microscopy; TLRs, Toll-like receptors; TNF-α, tumor necrosis factor-α; Zol, zoledronate.

Data Sharing Statement

All data are provided in the article and are available upon request from the corresponding author.

Acknowledgments

The work was supported by the National Program for Multidisciplinary Cooperative Treatment on Major Diseases (grant PKUSSNMP202007) and the Beijing Municipal Natural Science Foundation (grants 7192230 and 7202234).

Disclosure

The authors declare that no competing interest exists.

References

1. Ruggiero SL, Dodson TB, Aghaloo T, Carlson ER, Ward BB, Kademani D. American Association of Oral and Maxillofacial Surgeons' Position Paper on Medication-Related Osteonecrosis of the Jaws-2022 Update. *J Oral Maxillofac Surg*. 2022;80(5):920–943. doi:10.1016/j.joms.2022.02.008
2. Yarom N, Shapiro CL, Peterson DE, et al. Medication-Related Osteonecrosis of the Jaw: MASCC/ISOO/ASCO Clinical Practice Guideline. *J Clin Oncol*. 2019;37(25):2270–2290. doi:10.1200/JCO.19.01186
3. Endo Y, Kumamoto H, Nakamura M, et al. Underlying Mechanisms and Therapeutic Strategies for Bisphosphonate-Related Osteonecrosis of the Jaw (BRONJ). *Biol Pharm Bull*. 2017;40(6):739–750. doi:10.1248/bpb.b16-01020
4. Jiang A, Zhang Z, Qiu X, Guo Q. Medication-related osteonecrosis of the jaw (MRONJ): a review of pathogenesis hypothesis and therapy strategies. *Arch Toxicol*. 2024;98(3):689–708. doi:10.1007/s00204-023-03653-7
5. Ruan HJ, Li MY, Zhang ZY, Ma HL, He Y. Medication-related osteonecrosis of the jaw: a retrospective single center study of recurrence-related factors after surgical treatment. *Clin Oral Investig*. 2024;28(10):549. doi:10.1007/s00784-024-05911-z
6. Rodriguez-Lozano FJ, Onate-Sanchez R, Gonzalvez-Garcia M, et al. Allogeneic Bone Marrow Mesenchymal Stem Cell Transplantation in Tooth Extractions Sites Ameliorates the Incidence of Osteonecrotic Jaw-Like Lesions in Zoledronic Acid-Treated Rats. *J Clin Med*. 2020;9(6). doi:10.3390/jcm9061649
7. Yang G, Kim YN, Kim H, Lee BK. Effect of Human Umbilical Cord Matrix-Derived Mesenchymal Stem Cells on Bisphosphonate-Related Osteonecrosis of the Jaw. *Tissue Eng Regen Med*. 2021;18(6):975–988. doi:10.1007/s13770-021-00372-x

8. Kaibuchi N, Iwata T, Yamato M, Okano T, Ando T. Multipotent mesenchymal stromal cell sheet therapy for bisphosphonate-related osteonecrosis of the jaw in a rat model. *Acta Biomater*. 2016;42:400–410. doi:10.1016/j.actbio.2016.06.022
9. Matsuura Y, Atsuta I, Ayukawa Y, et al. Therapeutic interactions between mesenchymal stem cells for healing medication-related osteonecrosis of the jaw. *Stem Cell Res Ther*. 2016;7(1):119. doi:10.1186/s13287-016-0367-3
10. Nakao N, Nakayama T, Yahata T, et al. Adipose tissue-derived mesenchymal stem cells facilitate hematopoiesis in vitro and in vivo: advantages over bone marrow-derived mesenchymal stem cells. *Am J Pathol*. 2010;177(2):547–554. doi:10.2353/ajpath.2010.091042
11. Brennan MA, Renaud A, Guilloton F, et al. Inferior In Vivo Osteogenesis and Superior Angiogenesis of Human Adipose-Derived Stem Cells Compared with Bone Marrow-Derived Stem Cells Cultured in Xeno-Free Conditions. *Stem Cells Transl Med*. 2017;6(12):2160–2172. doi:10.1002/sctm.17-0133
12. Volarevic V, Markovic BS, Gazdic M, et al. Ethical and Safety Issues of Stem Cell-Based Therapy. *Int J Med Sci*. 2018;15(1):36–45. doi:10.7150/ijms.21666
13. Chang C, Yan J, Yao Z, Zhang C, Li X, Mao HQ. Effects of Mesenchymal Stem Cell-Derived Paracrine Signals and Their Delivery Strategies. *Adv Healthc Mater*. 2021;10(7):e2001689. doi:10.1002/adhm.202001689
14. Zhang Y, Liu Y, Liu H, Tang WH. Exosomes: biogenesis, biologic function and clinical potential. *Cell Biosci*. 2019;9:19. doi:10.1186/s13578-019-0282-2
15. Kalluri R, LeBleu VS. The biology, function, and biomedical applications of exosomes. *Science*. 2020;367(6478). doi:10.1126/science.aau6977
16. Pegtel DM, Gould SJ. Exosomes. *Annu Rev Biochem*. 2019;88:487–514. doi:10.1146/annurev-biochem-013118-111902
17. Tienda-Vazquez MA, Hanel JM, Marquez-Arteaga EM, et al. Exosomes: a Promising Strategy for Repair, Regeneration and Treatment of Skin Disorders. *Cells*. 2023;12(12). doi:10.3390/cells12121625
18. Watanabe J, Sakai K, Urata Y, Toyama N, Nakamichi E, Hibi H. Extracellular Vesicles of Stem Cells to Prevent BRONJ. *J Dent Res*. 2020;99(5):552–560. doi:10.1177/0022034520906793
19. Huang J, Wang L, Tian W. Small Extracellular Vesicles Derived from Adipose Tissue Prevent Bisphosphonate-Related Osteonecrosis of the Jaw by Promoting Angiogenesis. *Int J Nanomed*. 2021;16:3161–3172. doi:10.2147/IJN.S305361
20. Zheng Y, Dong X, Wang X, et al. Exosomes Derived from Adipose Tissue-Derived Mesenchymal Stromal Cells Prevent Medication-Related Osteonecrosis of the Jaw through IL-1RA. *Int J Mol Sci*. 2023;24(10). doi:10.3390/ijms24108694
21. Dong X, He L, Zang X, et al. Adipose-Derived Stem Cells Promote Bone Coupling in Bisphosphonate-Related Osteonecrosis of the Jaw by TGF-beta1. *Front Cell Dev Biol*. 2021;9:639590. doi:10.3389/fcell.2021.639590
22. Zang X, He L, Zhao L, He Y, Xiao E, Zhang Y. Adipose-derived stem cells prevent the onset of bisphosphonate-related osteonecrosis of the jaw through transforming growth factor beta-1-mediated gingival wound healing. *Stem Cell Res Ther*. 2019;10(1):169. doi:10.1186/s13287-019-1277-y
23. Yu P, Zhang X, Liu N, Tang L, Peng C, Chen X. Pyroptosis: mechanisms and diseases. *Signal Transduct Target Ther*. 2021;6(1):128. doi:10.1038/s41392-021-00507-5
24. Wei X, Xie F, Zhou X, et al. Role of pyroptosis in inflammation and cancer. *Cell Mol Immunol*. 2022;19(9):971–992. doi:10.1038/s41423-022-00905-x
25. Wei Y, Lan B, Zheng T, et al. GSDME-mediated pyroptosis promotes the progression and associated inflammation of atherosclerosis. *Nat Commun*. 2023;14(1):929. doi:10.1038/s41467-023-36614-w
26. Cai X, Zhang ZY, Yuan JT, et al. hucMSC-derived exosomes attenuate colitis by regulating macrophage pyroptosis via the miR-378a-5p/NLRP3 axis. *Stem Cell Res Ther*. 2021;12(1):416. doi:10.1186/s13287-021-02492-6
27. Baatarjav C, Komada T, Karasawa T, et al. dsDNA-induced AIM2 pyroptosis halts aberrant inflammation during rhabdomyolysis-induced acute kidney injury. *Cell Death Differ*. 2022;29(12):2487–2502. doi:10.1038/s41418-022-01033-9
28. Zhao P, Yue Z, Nie L, et al. Hyperglycaemia-associated macrophage pyroptosis accelerates periodontal inflamm-aging. *J Clin Periodontol*. 2021;48(10):1379–1392. doi:10.1111/jcpe.13517
29. Ao X, Yan H, Huang M, et al. Lavender essential oil accelerates lipopolysaccharide-induced chronic wound healing by inhibiting caspase-11-mediated macrophage pyroptosis. *Kaohsiung J Med Sci*. 2023;39(5):511–521. doi:10.1002/kjm2.12654
30. Sun S, Xu X, Liang L, et al. Lactic Acid-Producing Probiotic Saccharomyces cerevisiae Attenuates Ulcerative Colitis via Suppressing Macrophage Pyroptosis and Modulating Gut Microbiota. *Front Immunol*. 2021;12:777665. doi:10.3389/fimmu.2021.777665
31. Blevins HM, Xu Y, Biby S, Zhang S. The NLRP3 Inflammasome Pathway: a Review of Mechanisms and Inhibitors for the Treatment of Inflammatory Diseases. *Front Aging Neurosci*. 2022;14:879021. doi:10.3389/fnagi.2022.879021
32. Wu J, Lin S, Wan B, Velani B, Zhu Y. Pyroptosis in Liver Disease: new Insights into Disease Mechanisms. *Aging Dis*. 2019;10(5):1094–1108. doi:10.14336/AD.2019.0116
33. Wang C, Ma C, Gong L, et al. Macrophage Polarization and Its Role in Liver Disease. *Front Immunol*. 2021;12:803037. doi:10.3389/fimmu.2021.803037
34. Xu Y, Tang X, Fang A, et al. HucMSC-Ex carrying miR-203a-3p.2 ameliorates colitis through the suppression of caspase 11/4-induced macrophage pyroptosis. *Int Immunopharm*. 2022;110:108925. doi:10.1016/j.intimp.2022.108925
35. Hua T, Yang M, Song H, et al. Huc-MSCs-derived exosomes attenuate inflammatory pain by regulating microglia pyroptosis and autophagy via the miR-146a-5p/TRAF6 axis. *J Nanobiotechnology*. 2022;20(1):324. doi:10.1186/s12951-022-01522-6
36. Yan B, Zhang Y, Liang C, et al. Stem cell-derived exosomes prevent pyroptosis and repair ischemic muscle injury through a novel exosome/circHIPK3/ FOXO3a pathway. *Theranostics*. 2020;10(15):6728–6742. doi:10.7150/thno.42259
37. Kou X, Xu X, Chen C, et al. The Fas/Fap-1/Cav-1 complex regulates IL-1RA secretion in mesenchymal stem cells to accelerate wound healing. *Sci Transl Med*. 2018;10(432). doi:10.1126/scitranslmed.aai8524
38. Garlanda C, Dinarello CA, Mantovani A. The interleukin-1 family: back to the future. *Immunity*. 2013;39(6):1003–1018. doi:10.1016/j.immuni.2013.11.010
39. Isaac R, Reis FCG, Ying W, Olefsky JM. Exosomes as mediators of intercellular crosstalk in metabolism. *Cell Metab*. 2021;33(9):1744–1762. doi:10.1016/j.cmet.2021.08.006
40. Camussi G, Deregibus MC, Bruno S, Cantaluppi V, Biancone L. Exosomes/microvesicles as a mechanism of cell-to-cell communication. *Kidney Int*. 2010;78(9):838–848. doi:10.1038/ki.2010.278

41. Xia L, Zhang C, Lv N, et al. AdMSC-derived exosomes alleviate acute lung injury via transferring mitochondrial component to improve homeostasis of alveolar macrophages. *Theranostics*. 2022;12(6):2928–2947. doi:10.7150/thno.69533
42. Shen K, Jia Y, Wang X, et al. Exosomes from adipose-derived stem cells alleviate the inflammation and oxidative stress via regulating Nrf2/HO-1 axis in macrophages. *Free Radic Biol Med*. 2021;165:54–66. doi:10.1016/j.freeradbiomed.2021.01.023
43. Schroder K, Tschopp J. The inflammasomes. *Cell*. 2010;140(6):821–832. doi:10.1016/j.cell.2010.01.040
44. Li Y, Song W, Tong Y, et al. Isoliquiritin ameliorates depression by suppressing NLRP3-mediated pyroptosis via miRNA-27a/SYK/NF-kappaB axis. *J Neuroinflammation*. 2021;18(1):1. doi:10.1186/s12974-020-02040-8
45. Man SM, Karki R, Kanneganti TD. Molecular mechanisms and functions of pyroptosis, inflammatory caspases and inflammasomes in infectious diseases. *Immunol Rev*. 2017;277(1):61–75. doi:10.1111/imr.12534
46. Hsu CG, Chavez CL, Zhang C, Sowden M, Yan C, Berk BC. The lipid peroxidation product 4-hydroxynonenal inhibits NLRP3 inflammasome activation and macrophage pyroptosis. *Cell Death Differ*. 2022;29(9):1790–1803. doi:10.1038/s41418-022-00966-5
47. Rao Z, Zhu Y, Yang P, et al. Pyroptosis in inflammatory diseases and cancer. *Theranostics*. 2022;12(9):4310–4329. doi:10.7150/thno.71086
48. Kang R, Zeng L, Zhu S, et al. Lipid Peroxidation Drives Gasdermin D-Mediated Pyroptosis in Lethal Polymicrobial Sepsis. *Cell Host Microbe*. 2018;24(1):97–108e4. doi:10.1016/j.chom.2018.05.009
49. Lin LR, Gao ZX, Lin Y, et al. Akt, mTOR and NF-kappaB pathway activation in Treponema pallidum stimulates M1 macrophages. *Int Immunopharmacol*. 2018;59:181–186. doi:10.1016/j.intimp.2018.03.040
50. Wang S, Lin Y, Yuan X, Li F, Guo L, Wu B. REV-ERBalpha integrates colon clock with experimental colitis through regulation of NF-kappaB/NLRP3 axis. *Nat Commun*. 2018;9(1):4246. doi:10.1038/s41467-018-06568-5
51. Zhou L, Zhao H, Zhao H, et al. GBP5 exacerbates rosacea-like skin inflammation by skewing macrophage polarization towards M1 phenotype through the NF-kappaB signalling pathway. *J Eur Acad Dermatol Venereol*. 2023;37(4):796–809. doi:10.1111/jdv.18725
52. Kawai T, Akira S. Signaling to NF-kappaB by Toll-like receptors. *Trends Mol Med*. 2007;13(11):460–469. doi:10.1016/j.molmed.2007.09.002
53. Jimi E, Fei H, Nakatomi C. NF-kappaB Signaling Regulates Physiological and Pathological Chondrogenesis. *Int J Mol Sci*. 2019;20(24). doi:10.3390/ijms20246275
54. Ran Y, Su W, Gao F, et al. Curcumin Ameliorates White Matter Injury after Ischemic Stroke by Inhibiting Microglia/Macrophage Pyroptosis through NF-kappaB Suppression and NLRP3 Inflammasome Inhibition. *Oxid Med Cell Longev*. 2021;2021:1552127. doi:10.1155/2021/1552127
55. Voet S, Srinivasan S, Lamkanfi M, van Loo G. Inflammasomes in neuroinflammatory and neurodegenerative diseases. *EMBO Mol Med*. 2019;11(6). doi:10.15252/emmm.201810248
56. Zhu W, Xu R, Du J, et al. Zoledronic acid promotes TLR-4-mediated M1 macrophage polarization in bisphosphonate-related osteonecrosis of the jaw. *FASEB J Apr*. 2019;33(4):5208–5219. doi:10.1096/fj.201801791RR
57. Singla DK, Johnson TA, Tavakoli Dargani Z. Exosome Treatment Enhances Anti-Inflammatory M2 Macrophages and Reduces Inflammation-Induced Pyroptosis in Doxorubicin-Induced Cardiomyopathy. *Cells*. 2019;8(10). doi:10.3390/cells8101224
58. Petrasek J, Bala S, Csak T, et al. IL-1 receptor antagonist ameliorates inflammasome-dependent alcoholic steatohepatitis in mice. *J Clin Invest*. 2012;122(10):3476–3489. doi:10.1172/jci60777
59. Luan J, Zhang X, Wang S, et al. NOD-Like Receptor Protein 3 Inflammasome-Dependent IL-1β Accelerated ConA-Induced Hepatitis. *Front Immunol*. 2018;9:758. doi:10.3389/fimmu.2018.00758
60. Borghi M, De Luca A, Puccetti M, et al. Pathogenic NLRP3 Inflammasome Activity during Candida Infection Is Negatively Regulated by IL-22 via Activation of NLRC4 and IL-1Ra. *Cell Host Microbe*. 2015;18(2):198–209. doi:10.1016/j.chom.2015.07.004